ELSEVIER

Contents lists available at ScienceDirect

Composites Part A

journal homepage: www.elsevier.com/locate/compositesa





Exceptional dynamic compressive properties of bio-inspired three-dimensional interlocking graphene network reinforced copper matrix composites

Bowen Li^a, Dong Lin^b, Xiang Zhang^{a,*}, Dongdong Zhao^a, Chunnian He^{a,c,d,*}, Naiqin Zhao^{a,d}

- a School of Materials Science and Engineering, Tianjin Key Laboratory of Composite and Functional Materials, Tianjin University, Tianjin 300072, China
- ^b School of Mechanical, Industrial and Manufacturing Engineering, Oregon State University, Corvallis, OR 97331, USA
- c Joint School of National University of Singapore and Tianjin University, International Campus of Tianjin University, Binhai New City, Fuzhou 350207, China
- ^d Collaborative Innovation Center of Chemical Science and Engineering (Tianjin), Tianjin 300072, China

ARTICLE INFO

Keywords:

- A. Metal-matrix composites (MMCs)
- A. 3-Dimensional reinforcement
- B. Impact behavior
- C. Finite element analysis (FEA)

ABSTRACT

Insights into the reinforcement spatial architectures and their fundamental effects on the dynamic mechanical behaviors are of great importance for designing shock-resistant metallic structures. In this study, we report copper matrix composites (CMCs) reinforced by three-dimensional interlocking graphene network (3D-IGN) with a unique bio-inspired "brick-bridge-mortar" structure. Our results demonstrate that the 3D-IGN/Cu shows simultaneously enhanced dynamic strength and ductility as compared to the uniformly-distributed RGO/Cu and pure Cu at the specific strain rate from $1000~\rm s^{-1}$ to $8000~\rm s^{-1}$. The interlocking network structure not only blocks dislocation movement and restricts grain boundary sliding, but also alleviates the heat-induced softening by improving the thermal conductivity in the horizontal direction. The finite element simulation results further confirm the important role of the graphene network on strain delocalization. This work offers a promising bottom-up tactic to fabricate CMCs with network architecture and superior dynamic properties for high-rate applications.

1. Introduction

Owing to their excellent electrical and thermal conductivity, copper and its alloys are widely used in the areas such as transportation, aerospace, and electronics industries [1]. High strain rate deformation occurs in a variety of situations, such as high-speed cutting, wire drawing, vehicle collision, armor penetration, high speed air flow impact and so on [2,3], during the forming process and serving of copper-based components. The high strain rate circumstance requires high performance of the dynamic properties of the components [4]. The fraction of heat extracted becomes smaller as the increase of the strain rate during impact loading, leading to a sharp temperature rise and softening [5]. At sufficiently high rates of deformation, the extracted heat can be neglected, and one has an adiabatic condition [6]. It is reported that adiabatic shear bands (ASBs) prefer to nucleate in those alloys (e.g. Cu-Zn [7] and Cu-Al alloys [8]) with lower stacking fault energy, despite of the fact that more obvious hardening behavior was

dominated with decreasing stacking fault energy under quasi-static loading [9]. Undesirable pre-failure normally happens and therefore causes potentially harmful effects to the structural materials.

Graphene, with various excellent mechanical and physical properties, including high Young's modulus and tensile strength [10,11], and superior carrier mobility and thermal conductivity [12,13], has recently attracted much scientific interest in the field of composite materials [14,15]. The large aspect ratio as well as the flexible layered structure of graphene allows for more effective contact with the matrix and energy absorption [16], which makes it an ideal reinforcement for improving the dynamic properties of Cu matrix composites. Simulation results by Liu et al. revealed that the graphene/Cu interface has two properties: the weak bending stiffness of graphene results in interlayer reflections and weakening the shock waves, while the covalently-bonded sp² structures in graphene constrain the dislocations and heal the matrix [17]. Long et al. further validated that the orientations of the graphene/Cu interface perpendicular and parallel to the incident shocking waves play

E-mail addresses: zhangxiang@tju.edu.cn (X. Zhang), cnhe08@tju.edu.cn (C. He).

^{*} Corresponding authors at: School of Materials Science and Engineering, Tianjin Key Laboratory of Composite and Functional Materials, Tianjin University, Tianjin 300072, China (C. He).

diverse roles in the response of Cu microstructures [18]. Xiong et al. reported the dynamic mechanical properties of graphene/Cu system at strain rates up to $10^8 \ s^{-1}$, revealing the transition of the dislocation dominated deformation to twinning dominated deformation [19,20]. In the meantime, the theoretic results also confirm that the planar defects such as staking faults and nanotwins in the Cu matrix could coordinate the plastic deformation synergistically with graphene/Cu interface [18]. The above results indicated that the extraordinary dynamic properties of graphene/Cu could be achieved through reasonable structure design. However, the successful composite fabrication and the related high strain-rate dynamics of the graphene/Cu system is lack of research.

Reinforcement architecture design is one of the most effective strategies in modulating the mechanical and physical properties of the composite materials [21]. For example, Shuai et al. designed superaligned carbon nanotube/Cu composites, which exhibited significant increase in strength and current transportation properties compared to pure Cu [22]. Xiong et al. fabricated laminated graphene/Cu composites, showing simultaneous increase in strength and ductility [23]. Combing the simulation results and the experimental operation, Jiang et al. introduced the Cu matrix composites with high mechanical properties through in-situ synthesis of $TiB_{2p} + TiB_w$ network [24]. In the aspect of high strain-rate deformation, Liu et al. reported a delicatelydesigned quasi-continuous TiB_w + graphene hybrid network/Ti composites by powder metallurgy [25]. The in-situ grown TiB_w pinned the grain boundary and the incorporated graphene dissipated heat to avoid the formation of ASBs. In the last decades, the bio-inspired structures have been widely used in composite materials [26], among which the highly-organized "brick-and-mortar" structure in nacre has been deeplystudied and reckoned as one of the best templates for impact resistant materials [27]. More recently, the research carried by Zhao et al. indicated that the "bridge" structures between the laminated layers of nacre and its inspired materials play the determined role in affecting their dynamic properties [28]. In another word, the composites with "brickbridge-mortar" structural should have better dynamic properties than those with "brick-and-mortar" structure. We believe that a "brickbridge-mortar" interlocking graphene network structure in the Cu matrix will not only pose more effective pinning for the grain boundary sliding and grain rotation, but also helps to dissipate the energy more uniformly thus avoiding the catastrophic adiabatic shear deformation in the composites.

In this work, copper matrix composites reinforced by a bio-inspired "brick-bridge-mortar" 3D interlocking graphene network architecture (3D-IGN/Cu), were fabricated via a bottom-up assembly and in-situ synthesis strategy. The high strain rate (1000 s⁻¹-8000 s⁻¹) behaviors of 3D-IGN/Cu composites were studied via Hopkinson bar and postmortem analysis. The results revealed that the derived dynamic compressive flow strength of 3D-IGN/Cu increased synchronously with the increase of strain rates and was always higher than that of pure Cu and RGO/Cu under the same strain rate. The microstructure evolution of the 3D-IGN/Cu was studied in detail, showing a combined strong dislocation pinning capability and excellent in-plane thermal conductivity. This 3D-IGN/Cu demonstrated a unique plastic deformation mechanism different from the common viscous drag theory for high-strain rate deformation. The superior shock resistance property of 3D-IGN/Cu makes it an outstanding candidate for high-rate applications.

2. Experimental method

2.1. Sample preparation

3D-IGN/Cu bulk composites were synthesized via a bottom-up and in-situ synthesis method. In detail, 15.0 g of spherical Cu powders with an averaged particle size of 1.0 μm were ball milled in a stainless-steel mixing jar at a speed of 400 rpm for 3 h under the protection of argon atmosphere, with a mass ratio between the Cu powder and the stainless-steel milling ball of about 1:20. Then, 0.320 g sucrose was dissolved in

the hybrid solution of ethanol and water (20 mL/40 mL) and stirred for 30 min to obtain a uniform and transparent solution. Subsequently, 24.0 g Cu flakes were added into the solution under stirring, sonicated for 20 min and then heated at 80°C under constant magnetic stirring until the solution was fully vaporized. The evaporated hybrids were dried in a vacuum oven at 70°C for 3 h to remove residual solution and followed by grounding into powders. The precursor particles were then placed in a stainless-steel mold with a diameter of 30 mm and cold pressed (400 MPa, 3 min) into a green body block. Then, the block was placed into a tube furnace and calcined in an Ar-H₂ mixed atmosphere (Ar: 200 mL•min $^{-1}$; H₂: 100 mL•min $^{-1}$) with a holding temperature 900°C and incubation time of 1 h to in-situ synthesis 3D-IGN in the assembled Cu flakes template.

The calcinated bulk was placed in a graphite mold and then consolidated by hot-pressing at 950°C for 60 min with a pressure of 50 MPa, under a high vacuum level of 10^{-4} Pa level. The heating rate of hot-pressing was $10^{\circ}\text{C} \cdot \text{min}^{-1}$. The hot-pressed composites were then hot-rolled to a thin plate shape. The rolling reduction during each rolling cycle was 0.2 mm. After each pass, the samples were placed in a box furnace at 800°C for 2 min. For comparison, control samples made of pure Cu powder were also produced via the same process. As for RGO/Cu, GO was first dispersed in the ethanol solution by ultrasonication for half an hour. Then it followed the same densification steps as 3D-IGN/Cu to get the final bulk materials.

2.2. Quasi-static tensile and compression tests

A standard mechanical tester (Lloyd (AMETEK) EZ 20) was used to perform the quasi-static uniaxial tensile and compression tests. The tensile properties of dog-bone shape specimen with a gauge length of 10 mm, a gauge width of 3 mm and a thickness of 2 mm were prepared by wire cutting were tested at a rate of 0.5 mm \bullet min $^{-1}$. The compression tests were carried out at a strain rate of 0.001 s $^{-1}$ with cylinder-type specimens (Φ 1.5 mm \times 2 mm).

2.3. Dynamic compression tests

The dynamic compression tests were carried out by a split Hopkinson pressure bar (SHPB) setup, which consisted of a striker, an incident bar and a transmission bar. The cylindrical specimens (Φ 3 mm \times 3 mm) were sandwiched between the incident and transmitter bars with the same diameter of 10 mm and length of 160 cm. A 300 mm long striker bar was projected onto the incident bar using air pressures of 0.04, 0.09, 0.26 and 0.58 MPa, respectively, which corresponded to the strain rates of 1000, 2000, 4000 and 8000 s $^{-1}$. Three specimens were tested at each strain rate to assure the consistence of the test results. As the elastic compressive wave reached the interface between the specimen and incident bar, part of it was transmitted into the transmission bar through the specimen, while the rest was reflected back into the incident bar as elastic tensile waves. The strain pulses were recorded using strain gauges mounted on the transmission and incident bars.

2.4. Structure characterization

Post-mortem microstructural observations were carried out on a S-4800 SEM and JEM-2100F TEM respectively. Raman spectroscopy (Reinishaw inVia Reflex) was used to verify the crystallinity of 3D-IGN. EBSD was performed with a field-emission scanning electron microscope (SEM, Sigma 300) fitted with an EBSD detector. X-ray diffraction (XRD) was carried out with Cu K_{α} radiation (D8 Advance).

2.5. Finite element model

Finite element simulations were carried out based on ANSYS 19.2 software and the corresponding models were meshed using Solid 186 (3D20N). Based on the physical properties of the materials, the material

models of graphene network and Cu matrix are defined as Structural, Linear, Elastic and Isotropic in finite element analysis. The graphene layer thickness was 0.05 μm . The length and height of the 3D-IGN grid were 5 μm and 0.5 μm respectively, with the same graphene layer spacing used for the uniformly distributed laminated graphene/Cu model. A bonded contact was chosen as the interfacial binding of graphene and Cu. The parameters of graphene and Cu matrix are shown in Supplementary table S1. The models were compressed at a strain rate of 8000 s $^{-1}$ in the direction perpendicular to the graphene layer.

3. Result

B. Li et al.

3.1. Microstructural characterizations

As depicted in Fig. 1, to fabricate 3D-IGN/Cu, copper flakes obtained by ball milling of spherical copper powder with an average size of 1 μm were chosen as the building blocks for the assembly, acting as both the template and also the catalyst. Sucrose as the solid carbon source was coated on the surface of copper flakes by a convenient impregnation and drying method. The assembly of the hybrid precursors formed by cold-pressing was calcinated in a tube furnace, during which process 3D-IGN was in-situ constructed on the surface of the Cu flakes assembly. Unlike the traditional chemical vapor deposition strategy using the flat surface of Cu foils and Cu flakes as the substrate, in this work the Cu flakes assembly facilitated the growth of an interconnected network structure of graphene reinforcement. After further densification by hotpressing and hot-rolling, the 3D-IGN/Cu composites could be fabricated without the graphene agglomeration and debonding problems of the exsitu strategies.

Owing to the template of assembled Cu flakes, the complete network structure of 3D-IGN was exposed after etching the surface of the Cu matrix (Fig. 2a). The graphene in the composites demonstrates an anisotropic feature, with obvious alignment in the direction vertical to the pressing force while sparse connection with a much larger intervals in the parallel direction (Fig. 2b). After hot rolling deformation with 50% reduction in thickness, the interlocking graphene network could still be well preserved (Fig. 2c and d). From another point of view, the unique structure of IGN confines the Cu grains inside the network and thus it leads to a laminated Cu grain structure after hot-rolling spotted clearly from the TEM characterizations (Fig. 2e). Microscopically, The in-situ growth strategy not only solved graphene agglomeration issue but also facilitated to an intimate interfacial bonding between 3D-IGN and Cu [29]. The well-crystallized few-layer graphene (5–10 layers) has a layer spacing of 0.34 nm.

The Raman spectroscopy is an effective method to evaluate the evolution of the graphene structure during the fabrication process [30]. It is indicated that the hot-rolling deformation caused a slight structural damage to the quality of 3D-IGN, determined by the ratio (I_D/I_G)

between D band (1350 cm⁻¹) and G band (1580 cm⁻¹) changing from 0.85 to 0.95 after 50% deformation (Fig. 3a). Based on the microstructure characterization in Fig. 2c, d and Fig. S1, the structural integrity of 3D-IGN was maintained intact with little damage even after the severe deformation process: rolling deformation with 70% strain. Due to the reason of gas escaping and barrier of sintering by the graphene/Cu interface during the in-situ synthesis of 3D-IGN between the intervals of the Cu flake assemblies, voids and defects were formed in the bulk composites. However, this negative effect could be eliminated gradually by hot-rolling with the increase of the deformation degree [23]. The tensile test is an effective strategy to evaluate the densification of the sintered bulk metallic materials as both the strength and elongation are sensitive to the voids and defects in the specimens. From Fig. 3b, high tensile strength of 290 MPa and a moderate elongation of 7% were achieved after hot-rolling. The increased strength may be attributed to the reduction of the layer spacing of 3D-IGN in the direction parallel to the rolling plane as well as the increase of the density of the bulk samples. Different from the smashing of the rigid 3D reinforcement skeleton in the traditional interpenetrating composites after severe deformation [31], the "bridge" structure can be clearly identified from the Cu-etched surface of HR-70% (Fig. S1e and S9). It suggests that the good deformability of the flexible 3D-IGN structure coordinates the plastic deformation of the Cu matrix and restricts the grain size during the severe hot rolling process.

3.2. Dynamic compression properties

Typical dynamic compressive curves of 3D-IGN/Cu and pure Cu are shown in Fig. 4a and b. The flow stress, dynamic ductility, and energy absorbed by the specimen are calculated and listed in Table 1. A general trend under all loading conditions was established that the flow strength of the 3D-IGN/Cu composites was much higher than that of pure Cu at any strain rate from 1000 s⁻¹ to 8000 s⁻¹. As the strain rate increasing, the flow strength and the dynamic ductility of the material improved markedly at the same time. Note that even under a high strain rate of 4000 s⁻¹, 3D-IGN/Cu reached the dynamic compressive strength of 511 MPa and energy absorption of 611.2 MJ·m⁻³, which were 7% and 21% higher than that of pure Cu, respectively. For a higher strain rate of 8000 s⁻¹, the flow strength of 3D-IGN/Cu is still better than pure Cu. It suggests that softening mechanisms became dominated at this strain rate, which will be discussed in the following sections. Considering the anisotropic microstructure of 3D-IGN/Cu, we also tested the dynamic properties at the strain rate of 1000 s⁻¹ in the vertical direction. The result indicates the attenuated strengthening effect compared to that in the parallel direction (Fig.S2), which is caused by the sparse distribution of graphene nanosheets along this direction in the bulk composites. It is also worth mentioning that the dynamic ductility on the stress-strain curve is not the strain corresponding to the specimen fracture. The

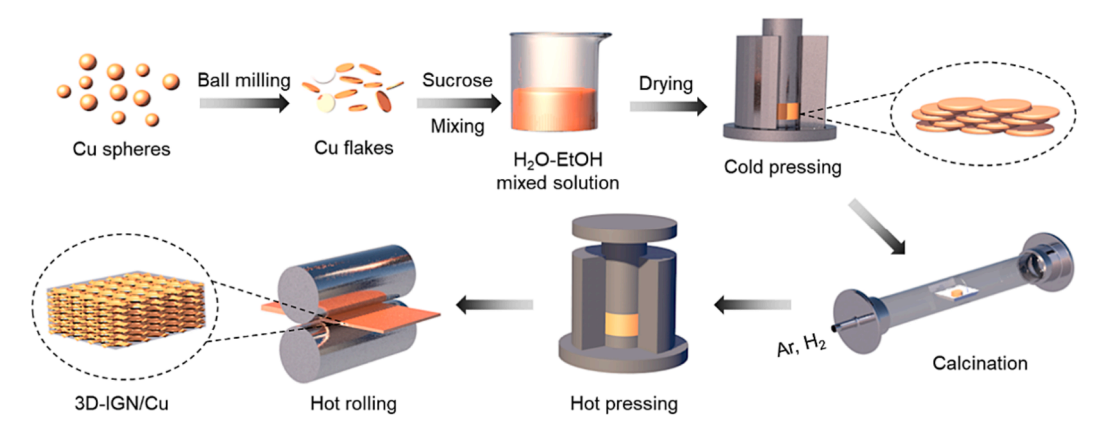


Fig. 1. Schematic illustration of the overall fabrication process of 3D-IGN/Cu.

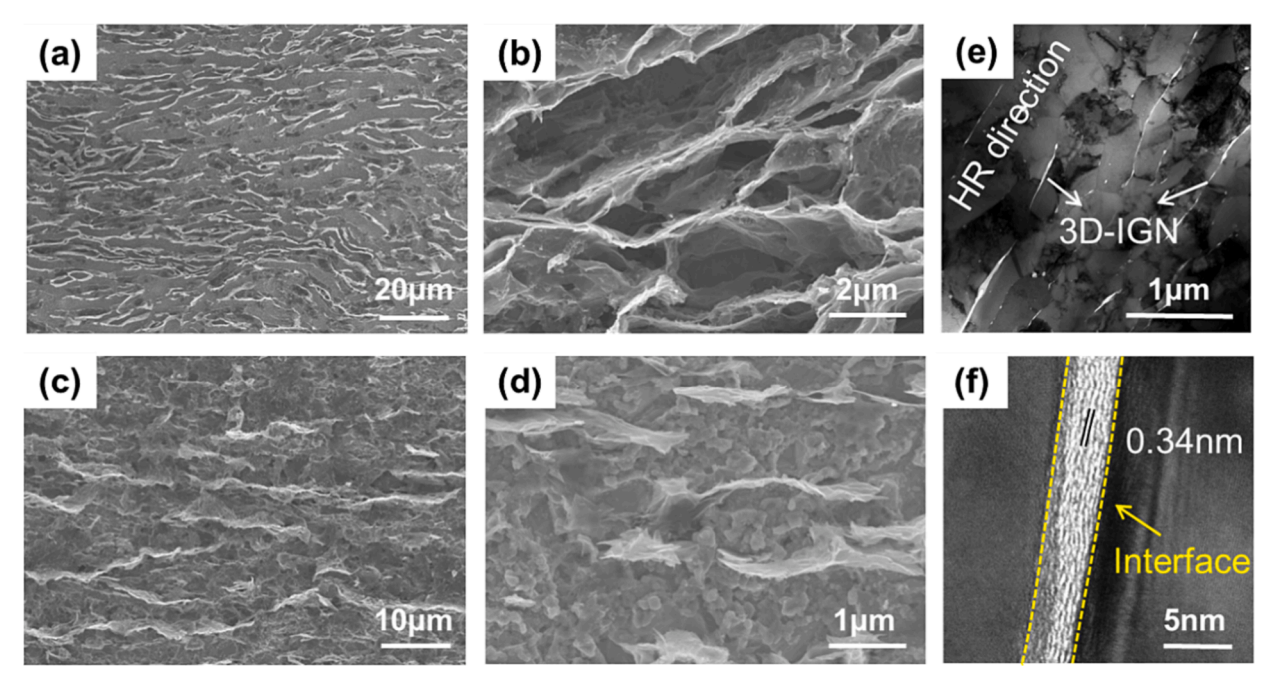


Fig. 2. Morphology characterizations of 3D-IGN/Cu bulk composites. SEM image of the graphene network morphology after Cu etching in the (a, b) hot-pressed 3D-IGN/Cu composites and (c, d) hot-rolled 3D-IGN/Cu composites. (e) TEM image of 3D-IGN in the hot-pressed composites. (f) Typical high resolution TEM image of interfacial areas in 3D-IGN/Cu.

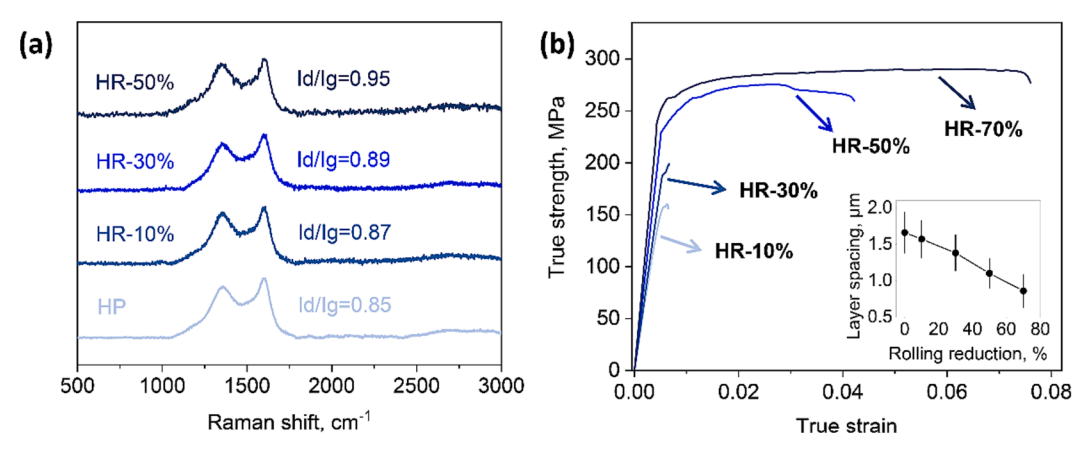


Fig. 3. (a) Raman spectra and (b) tensile stress-strain curves of 3D-IGN/Cu with different rolling deformation.

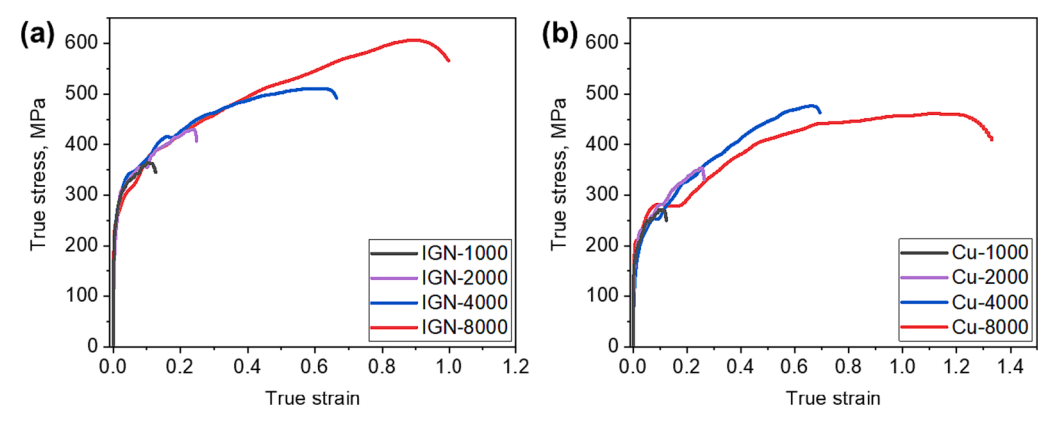


Fig. 4. Dynamic compressive stress-strain curves of (a) 3D-IGN/Cu and (b) pure Cu of different strain rate from 1000 s⁻¹ to 8000 s⁻¹.

Table 1
Strain rate, flow strength, dynamic ductility and absorbed energy per unit volume of 3D-IGN/Cu and pure Cu.

Sample	Strain rate (s ⁻¹)	Flow strength (MPa)	Dynamic ductility (%)	Energy absorb ($MJ \cdot m^{-3}$)
Cu	1000 2000 4000 8000	$\begin{array}{c} 271 \pm 2.1 \\ 354 \pm 7.1 \\ 476 \pm 8.1 \\ 470 \pm 1.5 \end{array}$	$\begin{aligned} &13.1 \pm 0.5 \\ &26.6 \pm 1.2 \\ &72.0 \pm 1.7 \\ &139 \pm 2.1 \end{aligned}$	37.2 ± 10.8 100.5 ± 7.1 502.4 ± 93.6 $2177.8 \pm$ 89.8
3D-IGN/ Cu	1000 2000 4000	364 ± 2.1 430 ± 7.5 511 ± 12.0	13.4 ± 0.3 25.2 ± 0.2 68.6 ± 1.6	49.3 ± 6.2 119.3 ± 2.0 611.2 ± 19.8
	8000	606 ± 9.7	108 ± 1.7	$1514.3 \pm \\58.3$

digital image of the specimen after dynamic compression, as shown in Fig. S3, indicates the good deformability of the composites without collapse. Compared to 3D-IGN/Cu, the homogeneously distributed RGO/Cu (as revealed in Fig. S4a) only exhibits a much lower flow strength as well as the dynamic ductility with the same weight ratio of graphene (Fig. S4b), suggesting that the spatial architecture of graphene plays an important role in affecting the final dynamic mechanical performance.

3.3. Post-shocking microstructure characterization

Shi et al. [32] previously reported that the 2D geometrical feature of

graphene caused a special strain state near the interface and thus provided the unique driving force for the abnormal grain growth in the graphene/Cu composites. The above mechanism works well in the RGO/ Cu with separately distributed graphene oxide sheets. However, the 3D-IGN/Cu shows a different mechanism. As depicted in Fig. 5a, the network structure had a strong pinning force on the grain growth of the Cu matrix, which causes a small average size of 0.45 µm. Even after a high strain rate deformation of 4000 s⁻¹ and 8000 s⁻¹, the grain sizes were controlled to be 0.62 μm and 0.45 μm without obvious change in the grain structure (Fig. 5b and c). The shear localization happened immediately after dynamic compression at 8000 s⁻¹, which causes the obvious recrystallization of the matrix grains. The severe coarsening phenomenon happened in RGO/Cu with average grain size 7.82 µm after hot-rolling deformation (Fig. S5). The significant difference between initial microstructure between RGO/Cu and 3D-IGN/Cu accounted for their varied impact behaviors as well as the structural stability during shocking deformation. The typical IPF figure of 3D-IGN before and after compression at 4000 s⁻¹ strain rate demonstrated negligible change. While severe shear deformation was revealed from RGO/Cu after 4000 s⁻¹ shocking deformation (Fig. S5b). For strain rate of 8000 s⁻¹, both the composites exhibited the similar recrystallization trend and rapid decrease of the ratio of the low-angle grain boundaries (LAGBs) as revealed form the distribution of grain boundary misorientations (Fig. 5d and Fig, S6). Moreover, the LAGBs ratio of the post-impact 3D-IGN/Cu increased to 25% suggests that the plastic deformation was still dominated by the dislocation behaviors rather than shear localization in RGO/Cu.

To have a close observation on the microstructure evolution of the

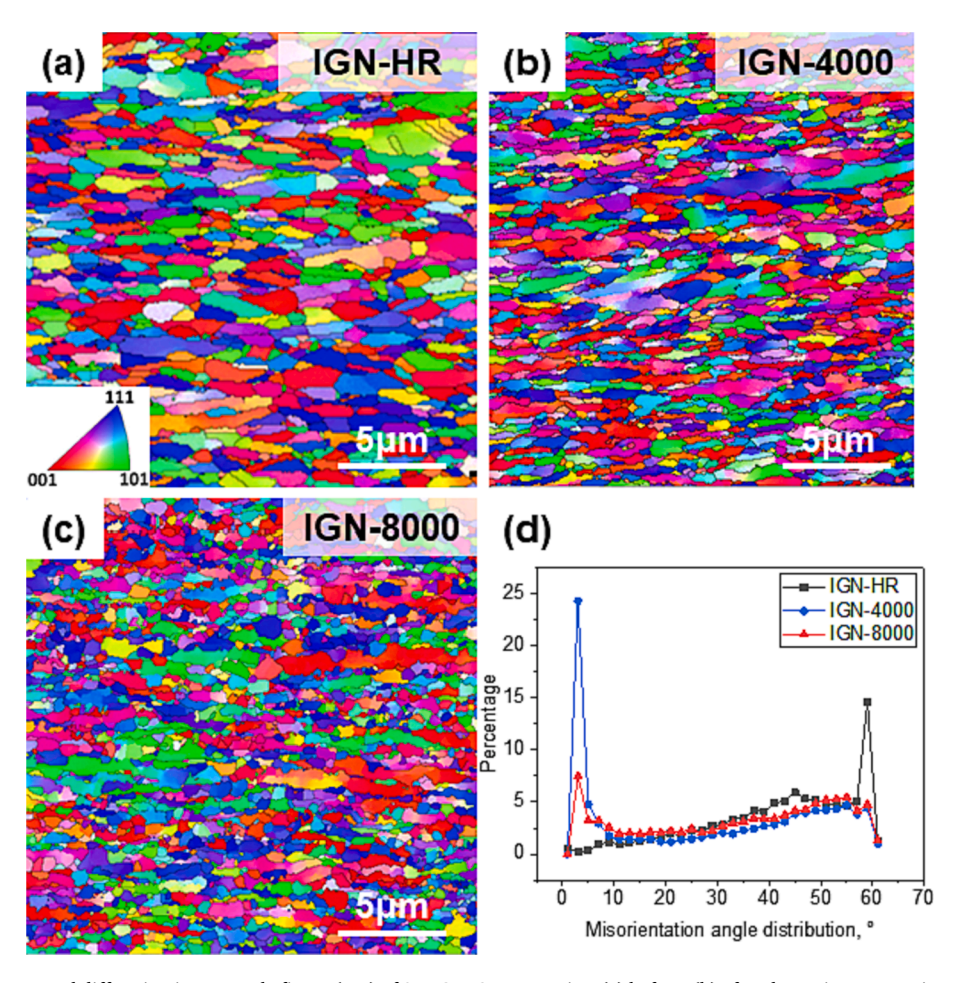


Fig. 5. The electron backscattered diffraction inverse pole figure (IPF) of 3D-IGN/Cu composites (a) before, (b) after dynamic compression at $4000 \, \text{s}^{-1}$ strain rate and (c) after dynamic compression at $8000 \, \text{s}^{-1}$ strain rate. (d) Difference in misorientation angle distribution of 3D-IGN/Cu before and after dynamic compression.

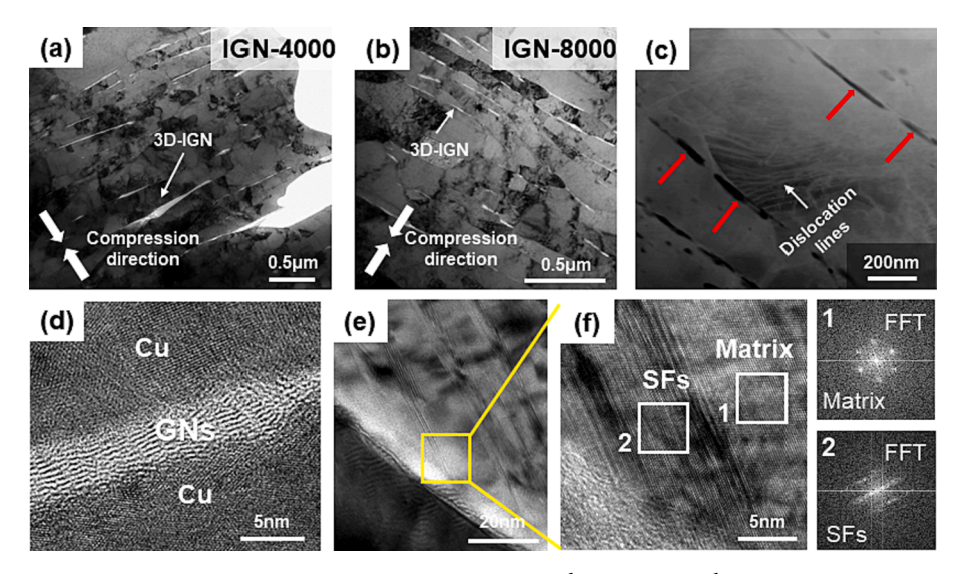


Fig. 6. TEM image of 3D-IGN/Cu after dynamic compression at the strain rate of (a) $4000 \, \text{s}^{-1}$ and (b) $8000 \, \text{s}^{-1}$. (c) HAADF image of dislocations pinned by graphene in 3D-IGN/Cu after dynamic compression after $8000 \, \text{s}^{-1}$ deformation. The red arrows indicated the intragranular distribution of graphene. (d) HRTEM of 3D-IGN/Cu interface after dynamic compression at $8000 \, \text{s}^{-1}$. (e) TEM and (f) HRTEM of stacking faults near graphene with FFT diffraction patterns of Matrix and SFs after $8000 \, \text{s}^{-1}$ deformation.

composites after shocking deformation, the TEM characterizations of the cross-section were further carried out (Fig. 6). In macroscopic view, after the high strain rate compression, the microstructure of the composites still maintained the laminated morphology while the graphene layer spacing became significantly smaller in IGN-8000 (Fig. 6b) than that of IGN-4000 (Fig. 6a) because of the large deformation strain. Especially, the percentage of the areas with dark contrast designated to the dislocation tanglement were almost the same. The graphene distributed at the grain boundaries blocks the dislocation movement and confines the dislocation lines within one grain without creating slip lines through multiple grains, thus avoiding the formation of adiabatic shear bands (ASBs) [7]. From a higher-magnification image of Fig. 6c, partial fracture of 3D-IGN was observed and it resulted in the intragranular distribution of the graphene nanosheets with smaller lateral size surrounded by the recrystallized Cu grains, as indicated by the red arrows. In traditional particle reinforced metal matrix composites, the dynamic mechanical properties under high strain rate were severely degraded by the poor interfacial bonding between reinforcement and the metal matrix [25]. Owing to the Cu-O-C bonding between the in-situ grown IGN and Cu, the bonding strength of IGN/Cu interface could be sufficient to withstand the shocking impact under high strain rate. Besides, the flexible nature of IGN could also transfer and relax the shock loading at the interface and thus eliminate the shear localization. Therefore, the interface remained intact even under a high strain rate up to 8000 s⁻¹ (Fig. 6d). In the microstructure after compression at a strain rate of 8000 s⁻¹, high-resolution TEM image (HRTEM, Fig. 6 e-f) shows that there were some streaks emanating from the graphene and terminating inside the grain, distinctly different from the matrix, which were judged to be stacking faults (SFs) after fast Fourier transform processing. Due to the pinning effect of the graphene interface, plastic deformation associated with dislocation mechanism was confined at the 3D-IGN/Cu interface, and high-density stacking faults generated for coordination when the local stress exceeds the critical pressure for twin nucleation under high strain rate. In the previous work of Lin et al., they validated by experiments and simulations that nanotwins were generated near the graphene/Fe interface after laser shock peening due to the shock waves interaction with graphene [33]. Peng et al. also presented deformation twinning in the laminated graphene/Cu near the interface after laserinduced projectile impact test [34]. The above two works both focused on the ultra-high strain rate above 10⁶ s⁻¹. While in this work, the SFs structures in the IGN-8000 suggested that the extreme confinement network structure facilitates the emission of Shockley partials from graphene/Cu interface under a relatively low strain rate $\sim 10^4~{\rm s}^{-1}$. The extension of the SFs also benefits to the coordination deformation and improve the structural stability of the composites.

4. Discussion

4.1. Strain rate sensitivity

The experimental results showed that 3D-IGN/Cu, RGO/Cu, and pure Cu all exhibited higher flow stresses under dynamic compression compared to quasi-static compression. In order to understand the underlying mechanism, the SRS values (m), reflecting the sensitivity of the flow stress to changes of strain rate, were first estimated for all materials, using stresses obtained at 2–10% offset strains with the following relationships [35,36]:

$$\mathbf{m} = \frac{\partial \ln \sigma}{\partial \ln \dot{\mathbf{e}}} = \frac{\ln(\sigma_{h}/\sigma_{l})}{\ln(\dot{\mathbf{e}}_{h}/\dot{\mathbf{e}}_{l})} \tag{1}$$

where σ and $\dot{\epsilon}$ are the flow stress and strain rate at a fixed strain. The subscripts h and l represent the high and low strain rate, respectively. The strain rate for quasi-static compression was 0.001 s⁻¹ and the stress-strain curves were shown in Fig. S7. The SRS values of pure Cu and IGN/Cu composites at different strains were exhibited in Fig. 7. It shows that, at a specific strain of 2% during the initiation stage of the plastic deformation, 3D-IGN/Cu exhibited higher SRS values than pure Cu. It is well-known that the SRS values of FCC metals are sensitive to the matrix grain size [37]. Theoretically, the nanocrystalline and ultrafine-grained materials present an elevated SRS with up to an order of magnitude compared to their coarse-grained counterparts. This effect was caused by the transformation of the deformation mechanism from dislocation sliding to grain boundary sliding, which increased the density of mobile dislocations and the long-range internal stress level in the matrix. As a result, the activation volume was reduced significantly in the bulk metals with fine grains [38].

Herein, the significant refinement of the IGN yielded to a small average grain size of 0.45 μ m, which is believed to be the dominant factor in the obtained high SRS values of 0.038–0.048. The gradual reduced trend of SRS with the strain rate increasing from 1000 s^{-1} to 8000 s^{-1} was attributed to the thermal activation mechanism [39]. For RGO/Cu and pure Cu, the SRS values were calculated as 0.002–0.02 and

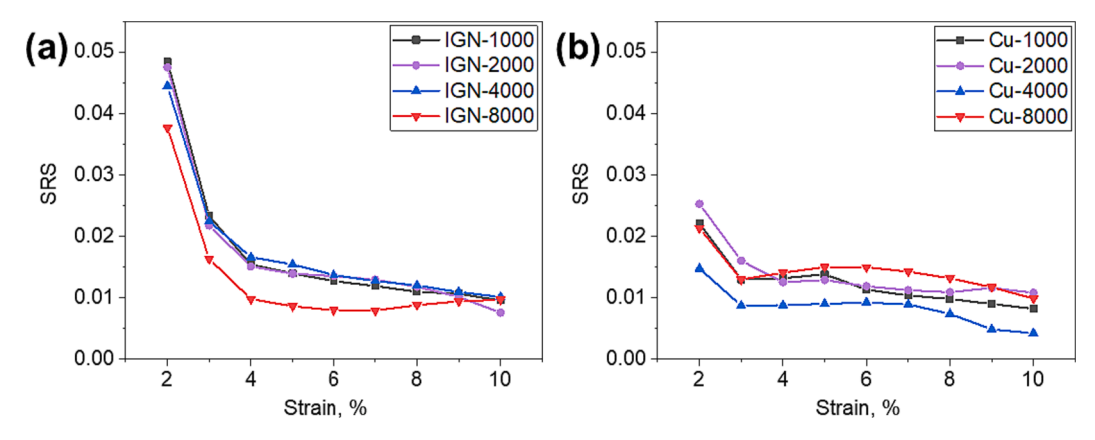


Fig. 7. The strain rate sensitivity of (a) 3D-IGN/Cu and (b) pure Cu at different plastic strains.

0.015–0.025 respectively, much lower than that of 3D-IGN/Cu. Besides, the SRS value of RGO/Cu first decreased with the strain rate increasing from $1000 \,\mathrm{s}^{-1}$ to $2000 \,\mathrm{s}^{-1}$ and then jumped to a higher value from 4000s⁻¹ to 8000 s⁻¹ (Fig. S8). It suggests that the change of the dominant rate-controlling deformation mechanism from thermal activation to viscous drag with the increase of the strain rate. While for pure Cu, a more complex changing trend for SHS values with the strain rate could be observed with a fluctuation near 0.02. The 3D-IGN/Cu did not follow the viscous drag mechanism which is supposed to plays a much more important role in the high strain rate deformation process. The classical theory of viscous drag mechanism suggests that dislocations moving freely through lattice experience a drag force from interactions with lattice vibrations when the dislocation is moving fast enough [40]. Previously, Casem et al. [41] and Srinivasan et al. [42] have separately demonstrated that the viscous drag could be well-controlled through the delicately-designed Ta particle distribution in the nanocrystalline Cu-Ta alloys. In this work, interlocking structure of 3D-IGN has a strong restriction on the grain boundary triple junction migration, which helps to increase the drag force during the high strain rate deformation process, leading to the inconspicuous viscous drag mechanism in 3D-IGN/Cu. On the contrary, the lacking of the efficient dislocation pinning mechanism in RGO/Cu and Cu results in the more significant increase in the flow strength with the increased strain rate, which is consistent with the Mayer's and Gillis's theory on the viscous drag behaviors [43,44]. In summary, the different response of the shocking treatment suggests that the spatial architecture of graphene plays an important part in the dynamic mechanical behaviors of the graphene/Cu composites.

4.2. Dislocation density

Overall, two important aspects govern dynamic deformation behavior, namely, the dislocation nucleation rate and the dislocation pinning/unpinning process. Due to the limited control of the position and the orientation of the reinforcement during preparation, the exact regulations based on experiments have been rarely reported on the dynamic properties of graphene reinforced metal matrix composites. Instead, the theoretical work based on the molecular dynamic (MD) simulations have achieved great breakthrough on the quasi-static and dynamic deformation mechanisms influenced by the graphene/copper interface, which provides the important preview for understanding the dislocation nucleation and pinning in the composite system. Numerous works have proved that the flexible nature of 2D graphene could enable the out-of-plane shape change during the matrix plastic deformation [17,18,45]. Specially, Long et al. revealed that under a high shocking force parallel to the one side of graphene/Cu interface may induce secondary dislocations on the other side via wrinkling of graphene, which enlarged the dislocation density in the bulk composites [18]. The simulation results suggested the possibility of regulating the dislocation

behaviors in the composites through the spatial architecture design of the graphene reinforcement. Compared to the laminated RGO/Cu, 3D-IGN/Cu is characterized by the "bridge" structure vertical to the graphene alignment direction [28]. The interlocking structure of the graphene network will cause different microstructure responses such as change in defect types, dislocation densities, grain boundary structures and so on.

Different thermal expansion coefficients and elastic modulus between the matrix and reinforcing phases nucleate geometric necessary dislocations (GND) during the rolling deformation and dynamic shocking tests [46]. Therefore, the dislocation density before and after shocking under different strain rates were firstly studied. Currently, indirect measurements of dislocation density using XRD are widely used, which could be determined by the X-ray line broadening of full-width at half maximum (FWHM) based on Williamson-Hal (W-H) method [47]. As displayed in Fig. 8, the dislocation density of 3D-IGN/Cu surpassed that of pure Cu and RGO/Cu before and after shocking deformation. For the hot-rolled composites, 3D-IGN has a strong pinning effect on the dislocation movement across the grain boundaries and the grain boundary migration, which could be verified indirectly by the uniform and equiaxed Cu grains. Furthermore, the good retaining of the 3D-IGN structure facilitates dislocation pinning effect and thus limits the grain migration and rotation trend [48]. The statistics of the dislocation density level of 2.2×10^{15} in 3D-IGN/Cu after 8000 s⁻¹ impact corresponds well with the TEM characterization results of the dislocation

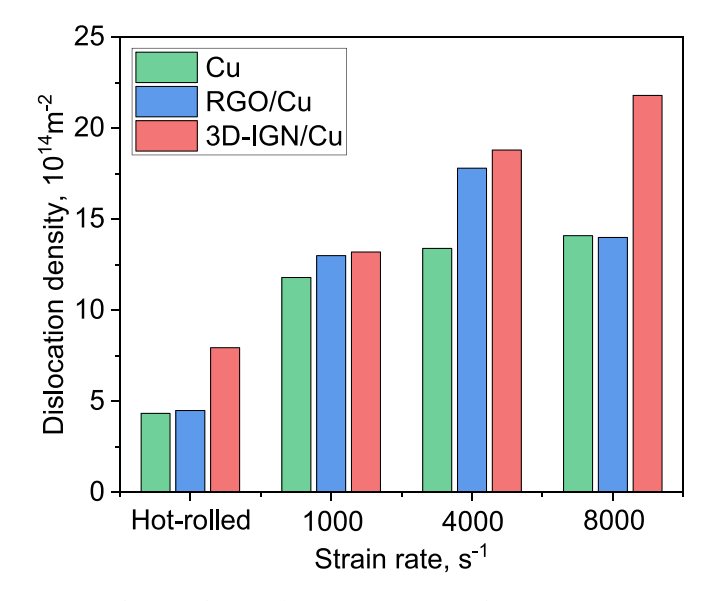


Fig. 8. Dislocation density of pure Cu, RGO/Cu and 3D-IGN/Cu composites before and after dynamic compression.

configuration in Fig. 6b. Comparatively speaking, the insensitive rise in dislocation with the increase of strain rate in pure Cu could be attributed to the thermal softening effect. As for RGO/Cu, the dislocation density reached the peak value of 1.8×10^{15} after shocking at $4000~\text{s}^{-1}$ but decreased to a low level almost equal to that of pure Cu after deformation at $8000~\text{s}^{-1}$. The results manifested that the softening mechanisms became dominant rather than strain hardening or strain rate hardening. Combined the results of strain rate sensitivity with the dislocation density, we conclude that the superb structural stability of 3D-IGN is the essential factor in achieving the excellent strain rate hardening properties in 3D-IGN/Cu.

4.3. Adiabatic temperature rise and thermal conductivity

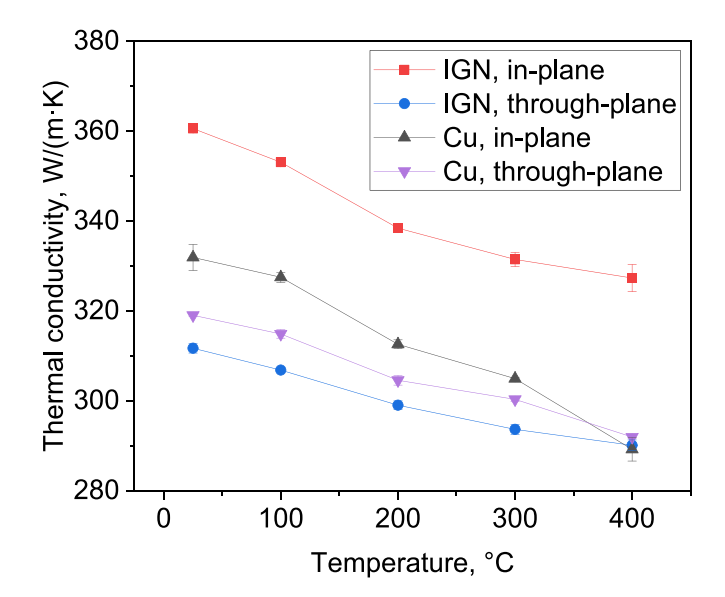
In the previously reported copper alloys, the high-strain-rate adiabatic deformation process leads to the accumulation of a large amount of heat in the material, which is difficult to dissipate instantly [7]. This often causes thermal softening effects in the local areas, dynamic recrystallization, and even catastrophic adiabatic shear bands. In metal matrix composites, this effect is often further amplified by the incorporation of a large number of heterogeneous interfaces [49]. On one hand, the thermal conductivity of ceramic particles is lower than that of the metal matrix, and it cannot effectively transfer heat away [50]. Moreover, the interfacial strength decreases at high temperature, leading to interface cracking and failure of the material under conditions of higher temperature and deformation rate compared to quasi-static deformation [51]. On the other hand, the localization effect will be more significant after thermal softening of the matrix under dynamic deformation conditions [52]. The formation of adiabatic shear bands will further exacerbate the incompatibility thus leading to matrix prefracture. In theory, the excellent thermal conductivity and flexible deformable characteristics of graphene are expected to greatly improve the above two effects in the graphene/Cu system.

Due to the very rapid deformation process during Hopkinson bar testing, the heat accumulated in the material is difficult to dissipate, which can lead to a temperature rise in the sample. The average temperature rise (ΔT) is estimated by the equation [31]:

$$\Delta T = \frac{n}{\rho c_p} \int_0^{\epsilon} \sigma d\epsilon \tag{2}$$

where n is the energy conversion coefficient (0.9 for copper alloy); $c_{\rm 0}$ and ρ are the specific heat and the density of the material, respectively; ϵ is the true strain. According to the above equation, the different theoretic temperature rises during the adiabatic high strain rate deformation process between 3D-IGN/Cu and RGO/Cu were mainly dependent on the absorbed energy. For example, the calculated average temperature rise of the 3D-IGN/Cu at $8000~s^{-1}$ was approximately calculated as 140 K, which is about 50 K higher than that of RGO/Cu (~90 K). Theoretically, the softening effect is more serious in 3D-IGN/Cu than RGO/Cu. In our experiments, however, neither obvious adiabatic shear band nor the abnormal grain behavior were observed in 3D-IGN/Cu. It evidenced that the adiabatic temperature rise effect could be offset by the network confinement effect as well as the efficient conductive channels for electrons and phonons in 3D-IGN structure.

To validate the above opinions, we measured the thermal conductivity of IGN/Cu from the two perpendicular directions. As demonstrated in Fig. 9 and Supplementary table S2, the thermal conductivity of 3D-IGN/Cu parallel to the rolling direction was 360.62 $W \cdot m^{-1} \cdot K^{-1}$, while in the vertical rolling direction the value was only 311.76 $W \cdot m^{-1} \cdot K^{-1}$. The results suggest that heat is conducted faster in the parallel direction than in the vertical direction which benefits the temperature homogenization in the composites during shocking deformation. Even under the high temperature up to 400°C, the thermal conductivity of 3D-IGN/Cu was higher than that of pure Cu in the parallel direction. It has been reported that both the directional arrangement of graphene in the Cu matrix and the low graphene/Cu interfacial



 $\textbf{Fig. 9.} \ \, \textbf{Thermal diffusivity of pure Cu and 3D-IGN/Cu composites at different temperatures.}$

thermal resistance lead to better in-plane thermal conductivity [53,54]. In the 3D-IGN/Cu composites, the graphene arrangement is highly parallel to the rolling direction (as shown in Fig. 2c), in the meantime the interface is tightly bonded without nano-voids (Fig. 2f), which resulted in a high in-plane thermal diffusivity [55]. In addition, the network architecture of graphene also helps to alleviate the anisotropy in thermal conduction, the thermal conductivity value of 3D-IGN/Cu in the vertical direction was almost on the same level as pure Cu. Therefore, the excellent thermal conductive behaviors of 3D-IGN/Cu could account for the offset negative impact of adiabatic temperature rise effect as commonly observed in the metal alloys.

4.4. FEM simulations

In the above discussions, we have validated that the unique deformation mechanism of 3D-IGN/Cu under the high-strain rate dynamic compression was caused by the efficient dislocation blocking effect of the network architecture. In order to further explore the effect of the architecture of graphene on the response of dynamic mechanical properties, we have simulated the dynamic compression behavior of 3D-IGN/ Cu and uniformly-dispersed laminated graphene/Cu using the finite element method, respectively. As illustrated in Fig. 10a and c, the difference of the simulated models lies in the distribution of graphene nanosheets in the direction parallel to the shocking direction in 3D-IGN/ Cu. Upon impact deformation at a strain rate of 8000 s⁻¹, the shock wave propagates in the Cu matrix and reflects between graphene layers, resulting in great difference on stress distributions in the bulk composites by comparing the snap shots of the compressive impact process (Figs. S10 and S11). For 3D-IGN/Cu, the stress distribution remains to be dispersed in the Cu matrix without identification of stress-concentrated areas (Fig. S10). While a clear trend of shear deformation at 45° to the incidence direction for homogeneously dispersed laminated graphene/ Cu (Fig. S11). The simulation results in Fig. 10b, d and S12 reveal that a higher stress level, which is more than 2.4 times, are observed in 3D-IGN/Cu compared to the uniformly dispersed laminated graphene/Cu. This difference mainly originates from the different architecture of graphene. In 3D-IGN/Cu, the two types of graphene in the orthogonal direction perform differently when the shock waves are applied on the graphene network. First, graphene can act as a dampener when the 3D-IGN/Cu interface is perpendicular to the shock wave (Fig. 11a and b). Second, the impact energy can be dispersed radially in the graphene layers, which were confirmed to possess good damping behaviors as

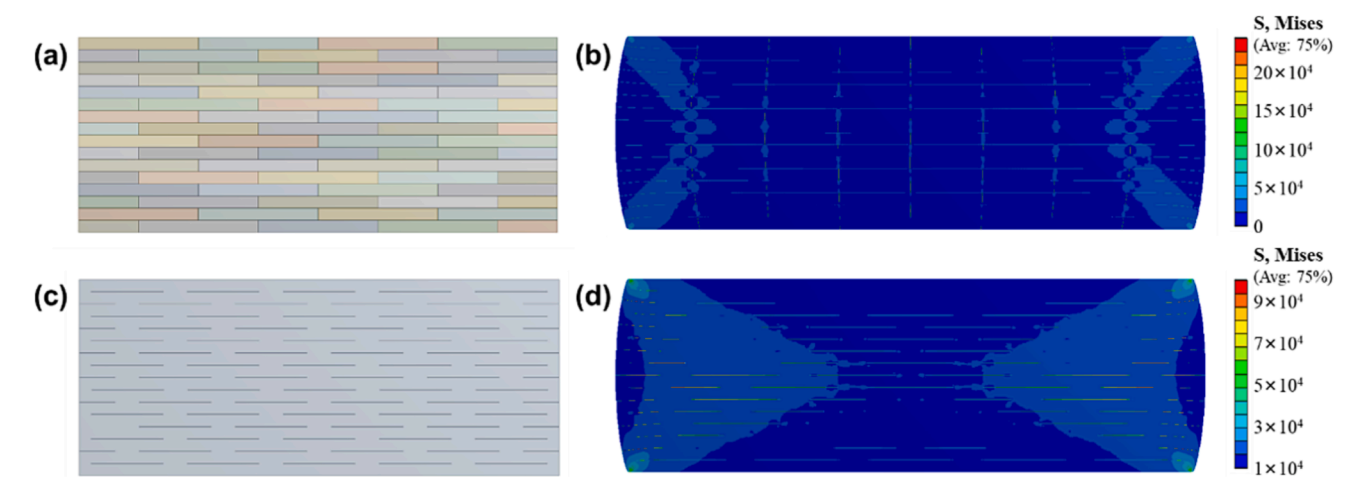


Fig. 10. Initial model and dynamic compression stress clouds for (a, b) 3D-IGN/Cu and (c, d) homogeneously dispersed laminated graphene/Cu in the finite element method.

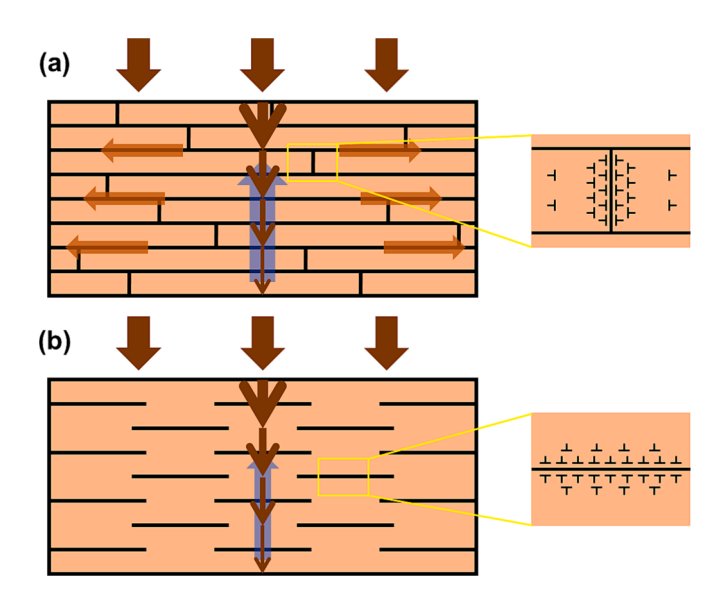


Fig. 11. Illustration of the interaction between shock waves and graphene interfaces in (a) 3D-IGN/Cu and (b) uniformly-dispersed laminated graphene/Cu.

reported [17]. Moreover, scattering at the interface leads to multiple reflections of the shock wave between the layers. These interactions between graphene and shock waves can effectively reduce the damage to the material from high strain rate compression. In the direction parallel to shock wave, graphene serves as the load barrier of the shocking stress and affects the stress distribution in the composites by alleviating the stress level in the graphene alignment direction. The high-stress areas in the uniformly-dispersed laminated graphene/Cu model presented an obvious extending trend at 45° to the laminated direction with severe stress concentration in the vicinity of the individual graphene nanosheets. However, diverse and less high stress areas were observed in 3D-IGN/Cu. The average stress level of the graphene nanosheets in the parallel direction was much higher than that in the vertical direction. The FEM simulation results aligns well with the experimental characterization and the dynamic mechanical behaviors is different between 3D-IGN/Cu and RGO/Cu. The elevated stress level in the direction parallel direction to the shocking wave may be caused by the increased dislocation density originated from the nucleation and propagation of the secondary-dislocations thus strengthened the matrix and reduced the risk of pre-cracking after shocking impact (as illustrated in Fig. 11b). The above results demonstrate that the great advantage of network

architecture design of graphene in resisting high-strain rate deformation.

Based on above experimental and FEM simulation results, the excellent dynamic compression properties of 3D-IGN/Cu can be associated with the following aspects: First, the continuous network structure of 3D-IGN restrains the Cu grains effectively [56], thus resulting ultrafined grain sizes with a high-level of SRS value in the bulk composites. Besides, owing to the great dislocation blocking capability of the network structure [57], the SRS value of 3D-IGN/Cu showed an abnormal negative changing trend with the increase of strain rate, without being affected by viscous drag mechanism in normal conditions. Second, the continuous network skeleton as well as the intimately bonded interface benefits to a superior thermal conductivity in the graphene alignment direction of 3D-IGN/Cu. The conductive channels can release the thermal rise effect during the adiabatic shocking process, lowering the possibility for the hazardous thermal softening and recrystallization. Last but not least, the "bridge-like" structure of 3D-IGN parallel to the dynamic compression directions promotes the nucleation and storage of the secondary-dislocations in its vicinity. It offers an efficient solution to disperse the stress distribution, thus avoiding the strain localization and improving both the flow strength and the dynamic ductility. Because of all above advantages, 3D-IGN/Cu exhibited a marvelous impact-resistant capability superior to the pure Cu and RGO/

5. Conclusions

In summary, the bio-inspired "brick-bridge-mortar" threedimensional interlocking graphene network reinforced copper matrix composites (3D-IGN/Cu) were fabricated through a powder-metallurgy method. The high strain rate (1000 s⁻¹ to 8000 s⁻¹) dynamic compressive deformation behaviors were studied in detail. The results revealed that at strain rate of 4000 s^{-1} , 3D-IGN/Cu showed a high-level dynamic compressive strength of 511 MPa and energy absorb of 611.2 MJ·m⁻³, which were 7% and 21% higher than that of pure Cu, respectively, with negligible change of its microstructure. At a higher strain rate of 8000 S⁻¹, high-density stacking faults were observed in the vicinity of graphene/Cu interface to coordinate the plastic deformation and avoid the strain localization. Contrary to the commonly positiverelated trend of metallic materials with an ultrafined grain size, 3D-IGN/Cu demonstrates a gradual decrease in the value of strain rate sensitivity with the rise of compression strain rate. The great dislocation blocking effect of the interlocking network and the good thermal conductivity of 3D-IGN/Cu in the parallel direction contributed to the strain delocalization, which stabilized the composites microstructure and

B. Li et al. Composites Part A 176 (2024) 107856

facilitated good strength and ductility during the dynamic compressive deformation. Furthermore, the FEM simulation result also confirmed the unique role of "bridge" structure in dispersing stress waves and strengthening the composites. This work highlighted the great potential of graphene architecture design for achieving extraordinary shock resistant properties.

CRediT authorship contribution statement

Bowen Li: Writing – original draft, Data curation, Investigation. **Dong Lin:** Visualization, Resources. **Xiang Zhang:** Writing – review & editing, Supervision, Funding Acquisition, Project administration. **Dongdong Zhao:** Formal analysis, Conceptualization. **Chunnian He:** Writing – review & editing, Supervision, Funding Acquisition, Project administration. **Naigin Zhao:** Formal analysis, Conceptualization.

Declaration of Competing Interest

The authors declare that they have no known competing financial interests or personal relationships that could have appeared to influence the work reported in this paper.

Data availability

Data will be made available on request.

Acknowledgments

The authors gratefully acknowledge the financial support by the National Natural Science Foundation of China, China (Grant No. 52101181, 52130105), the Chinese National Natural Science Fund for Distinguished Young Scholars (Grant No. 52025015), and the National Science Foundation, United States under Award No. 1943445.

Appendix A. Supplementary material

Supplementary data to this article can be found online at https://doi.org/10.1016/j.compositesa.2023.107856.

References

- [1] Lu L, Shen Y, Chen X, Qian L, Lu K. Ultrahigh strength and high electrical conductivity in copper. Science 2004;304(5669):422–6.
- [2] Yan N, Li ZZ, Xu YB, Meyers MA. Shear localization in metallic materials at high strain rates. Prog Mater Sci 2021;119:100755.
- [3] Cao Y, Ni S, Liao XZ, Song M, Zhu YT. Structural evolutions of metallic materials processed by severe plastic deformation. Mat Sci Eng R-Rep 2018;133:1–59.
- [4] Song KX, Geng YF, Ban YJ, Zhang Y, Li Z, Mi XJ, et al. Effects of strain rates on dynamic deformation behavior of Cu-20Ag alloy. J Mater Sci Technol 2021;79: 75–87.
- [5] Mishra A, Martin M, Thadhani N, Kad B, Kenik EA, Meyers M. High-strain-rate response of ultra-fine-grained copper. Acta Mater 2008;56(12):2770–83.
- [6] Wang Y, Liu Q, Zhang B, Zhang H, Zhong Z, Ye J, et al. Mechanical response and damage evolution of bio-inspired B4C-reinforced 2024Al composites subjected to quasi-static and dynamic loadings. Mat Sci Eng A-Struct 2022;840:142991.
- [7] Li J, Li Y, Huang C, Suo T, Wei Q. On adiabatic shear localization in nanostructured face-centered cubic alloys with different stacking fault energies. Acta Mater 2017; 141:163–82.
- [8] Chavan NM, Phani PS, Ramakrishna M, Venkatesh L, Pant P, Sundararajan G. Role of stacking fault energy (SFE) on the high strain rate deformation of cold sprayed Cu and Cu-Al alloy coatings. Mat Sci Eng A-Struct 2021;814:141242.
- [9] Hamdi F, Asgari S. Influence of stacking fault energy and short-range ordering on dynamic recovery and work hardening behavior of copper alloys. Scr Mater 2010; 62(9):693-6.
- [10] Novoselov KS, Geim AK, Morozov SV, Jiang DE, Zhang Y, Dubonos SV, et al. Electric field effect in atomically thin carbon films. Science 2004;306(5696): 666–9.
- [11] Novoselov KS, Fal' ko VI, Colombo L, Gellert PR, Schwab MG, Kim K. A roadmap for graphene. Nature 2012;490(7419):192-200.
- [12] Lee C, Wei X, Kysar JW, Hone J. Measurement of the elastic properties and intrinsic strength of monolayer graphene. Science 2008;321(5887):385–8.
- [13] Geim AK, Novoselov KS. The rise of graphene. Nat Mater 2007;6(3):183-91.

[14] Zhang Z, Fan G, Tan Z, Zhao H, Xu Y, Xiong D, et al. Bioinspired multiscale Al2O3rGO/Al laminated composites with superior mechanical properties. Compos B Eng 2021;217:108916.

- [15] Pu B, Zhang X, Chen X, Lin X, Zhao D, Shi C, et al. Exceptional mechanical properties of aluminum matrix composites with heterogeneous structure induced by in-situ graphene nanosheet-Cu hybrids. Compos B Eng 2022;234:109731.
- [16] Lahiri D, Das S, Choi WB, Agarwal A. Unfolding the damping behavior of multilayer graphene membrane in the low-frequency regime. ACS Nano 2012;6(5): 3992–4000.
- [17] Liu XY, Wang FC, Wu HA, Wang WQ. Strengthening metal nanolaminates under shock compression through dual effect of strong and weak graphene interface. Appl Phys Lett 2014;104(23):231901.
- [18] Long XJ, Li B, Wang L, Huang JY, Zhu J, Luo SN. Shock response of Cu/graphene nanolayered composites. Carbon 2016;103:457–63.
- [19] Peng YF, Luo GH, Hu YX, Xiong DB. Dynamic deformation mechanism in submicrolaminated copper with interlamellar graphene multilayers. Acta Mater 2023;252: 118941.
- [20] Peng YF, Luo GH, Chen JY, Hu YX, Xiong DB. Enhanced energy dissipation of graphene/Cu nanolaminates under extreme strain rate ballistic perforation. Compos A Appl S 2023;172:107611.
- [21] Lin Z, Zhang S, Ren L, Shen Z, Tang G, Shi P, et al. Enhanced strength and toughness of Ni/graphene composite via three-dimensional graphene-like nanosheets network. Compos B Eng 2023;253(15):110499.
- [22] Shuai J, Xiong LQ, Zhu L, Li WZ. Enhanced strength and excellent transport properties of a superaligned carbon nanotubes reinforced copper matrix laminar composite. Compos A Appl S 2016;88:148–55.
- [23] Cao M, Xiong DB, Tan ZQ, Ji G, Amin-Ahmadi B, Guo Q, et al. Aligning graphene in bulk copper: Nacre-inspired nanolaminated architecture coupled with in-situ processing for enhanced mechanical properties and high electrical conductivity. Carbon 2017;117:65–74.
- [24] Liu N, Zhang QQ, Zhang HY, Cao F, Feng PF, Zuo YF, et al. Experimental verification and numerical analysis on plastic deformation and mechanical properties of the in-situ TiB2 homogeneous composites and TiB2/Cu network composites prepared by powder metallurgy. J Alloy Compd 2022;920:165897.
- [25] Liu L, Li Y, Zhang H, Cheng X, Mu X, Ge Y. Breaking through the dynamic strength-ductility trade-off in TiB reinforced Ti composites by incorporation of graphene nanoplatelets. Compos B Eng 2022;230:109499.
- [26] Wegst UGK, Bai H, Saiz E, Tomsia AP, Ritchie RO. Bioinspired structural materials. Nat Mater 2015;14(1):23–36.
- [27] Yang W, Chen IH, Gludovatz B, Zimmermann EA, Ritchie RO, Meyers MA. Natural flexible dermal armor. Adv Mater 2013;25(1):31–48.
- [28] Zhao HW, Yue YH, Guo L, Wu JT, Zhang YW, Li XD, et al. Cloning nacre's 3D interlocking skeleton in engineering composites to achieve exceptional mechanical properties. Adv Mater 2016;28(25):5099–105.
- [29] Zhang X, Shi C, Liu E, Zhao N, He C. Effect of interface structure on the mechanical properties of graphene nanosheets reinforced copper matrix composites. ACS Appl Mater Inter 2018;10(43):37586–601.
- [30] Ferrari AC, Meyer JC, Scardaci V, Casiraghi C, Lazzeri M, Mauri F, et al. Raman spectrum of graphene and graphene layers. Phys Rev Lett 2006;97(18):187401.
- [31] Schukraft J, Horny D, Schulz K, Weidenmann KA. 3D modeling and experimental investigation on the damage behavior of an interpenetrating metal ceramic composite (IMCC) under compression. Mat Sci Eng A 2022;844:143147.
- [32] Shi HL, Gan WM, Esling C, Wang XJ, Zhang YD, Maawad E, et al. Elastic strain induced abnormal grain growth in graphene nanosheets (GNSs) reinforced copper (Cu) matrix composites. Acta Mater 2020;200:338–50.
- [33] Lin D, Motlag M, Saei M, Jin SY, Rahimi RM, Bahr D, et al. Shock engineering the additive manufactured graphene-metal nanocomposite with high density nanotwins and dislocations for ultra-stable mechanical properties. Acta Mater 2018;150:360–72.
- [34] Peng Y, Luo G, Hu Y, Xiong DB. Extreme strain rate deformation of nacre-inspired graphene/copper nanocomposites under laser-induced hypersonic micro-projectile impact. Compos B Eng 2022;235:109763.
- [35] Wei Q, Cheng S, Ramesh K, Ma E. Effect of nanocrystalline and ultrafine grain sizes on the strain rate sensitivity and activation volume: fcc versus bcc metals. Mat Sci Eng A-Struct 2004;381(1–2):71–9.
- [36] Wei Q. Strain rate effects in the ultrafine grain and nanocrystalline
- regimes—influence on some constitutive responses. J Mater Sci 2007;42:1709–27. [37] Mao ZN, An XH, Liao XZ, Wang JT. Opposite grain size dependence of strain rate
- [37] Mao ZN, An XH, Liao XZ, Wang JT. Opposite grain size dependence of strain rate sensitivity of copper at low vs high strain rates. Mat Sci Eng A 2018;738:430–8.
- [38] Fu XW, Xu R, Yuan C, Tan ZQ, Fan GL, Ji G, et al. Strain rate sensitivity and deformation mechanism of carbon nanotubes reinforced aluminum composites. Metal Mater Trans A 2019;50:3544–54.
- [39] Suo T, Li YL, Zhao F, Fan XL, Guo WG. Compressive behavior and rate-controlling mechanisms of ultrafine grained copper over wide temperature and strain rate ranges. Mech Mater 2013;61:1–10.
- [40] Park JM, Moon J, Bae JW, Jang MJ, Park J, Lee S, et al. Strain rate effects of dynamic compressive deformation on mechanical properties and microstructure of CoCrFeMnNi high-entropy alloy. Mat Sci Eng A 2018;719:155–63.
- [41] Casem D, Ligda J, Walter T, Darling K, Hornbuckle B. Strain-rate sensitivity of nanocrystalline Cu-10Ta to 700,000/s. J Dynam Behav Mat 2020;6(1):24–33.
- [42] Srinivasan S, Sharma S, Turnage S, Hornbuckle BC, Kale C, Darling KA, et al. Role of tantalum concentration, processing temperature, and strain-rate on the mechanical behavior of copper-tantalum alloys. Acta Mater 2021;208:116706.
- [43] Meyers MA. Dynamic behavior of materials. John wiley & sons; 1994.
- [44] Gillis PP, Gilman JJ, Taylor JW. Stress dependences of dislocation velocities. Phil Mag 1969;20(164):279–89.

- [45] Wu YC, Shao JL, Zhan HF. Damage and self-healing characteristics of monolayer graphene enhanced Cu under ballistic impact. Mech Mater 2021;155:103736.
- [46] Arsenlis A, Parks DM. Crystallographic aspects of geometrically-necessary and statistically-stored dislocation density. Acta Mater 1999;47(5):1597–611.
- [47] Dorset D. X-ray diffraction: a practical approach. Microsc Microanal 1998;4(5): 513–5.
- [48] Nan N, Li JM, X Zhang, DD Zhao, Zhu FL, He CN, et al. Achieving excellent thermal stability in continuous three-dimensional graphene network reinforced copper matrix composites. Carbon;212:118153.
- [49] Bao G, Lin Z. High strain rate deformation in particle reinforced metal matrix composites. Acta Mater 1996;44(3):1011–9.
- [50] Hong Y, Chen XL, Wang WF, Wu YC. Microstructure and properties of SiC particles reinforced copper based alloy composite. Mod Phys Lett B 2013;27(19):1341025.
- [51] Wang Y, Xu X, Zhao WX, Li N, McDonald SA, Chai Y, et al. Damage accumulation during high temperature fatigue of Ti/SiCf metal matrix composites under different stress amplitudes. Acta Mater 2021;213:116976.

- [52] Osovski S, Rittel D, Venkert A. The respective influence of microstructural and thermal softening on adiabatic shear localization. Mech Mater 2013;56:11–22.
- [53] Chu K, Wang XH, Wang F, Li YB, Huang DJ, Liu H, et al. Largely enhanced thermal conductivity of graphene/copper composites with highly aligned graphene network. Carbon 2018;127:102–12.
- [54] Guo S, Zhang X, Shi C, Liu E, He C, He F, et al. In situ synthesis of high content graphene nanoplatelets reinforced Cu matrix composites with enhanced thermal conductivity and tensile strength. Powder Technol 2020;362:126–34.
- [55] Brillon A, Heintz JM, Constantin L, Pillier F, Lu YF, Silvain JF, et al. Anisotropic thermal conductivity and enhanced hardness of copper matrix composite reinforced with carbonized polydopamine. Compos Commun 2022;33:101210.
- [56] Zhang X, Xu Y, Wang M, Liu E, Zhao N, Shi C, et al. A powder-metallurgy-based strategy toward three-dimensional graphene-like network for reinforcing copper matrix composites. Nat Commun 2020;11(1):2775.
- [57] Zhang X, Shi C, Liu E, He F, Ma L, Li Q, et al. Achieving high strength and high ductility in metal matrix composites reinforced with a discontinuous threedimensional graphene-like network. Nanoscale 2017;9(33):11929–38.